Inorganic Chemistry

Article

pubs.acs.org/IC

Synthesis and Molecular Structure of Gold Triarylcorroles

Kolle E. Thomas,[†] Abraham B. Alemayehu,[†] Jeanet Conradie,[†,‡] Christine Beavers,[§] and Abhik Ghosh*[,†]

[†]Department of Chemistry, University of Tromsø, 9037 Tromsø, Norway

[‡]Department of Chemistry, University of the Free State, 9300 Bloemfontein, Republic of South Africa

[§]Advanced Light Source, Lawrence Berkeley National Laboratory, Berkeley, California 94720-8229, United States

Supporting Information

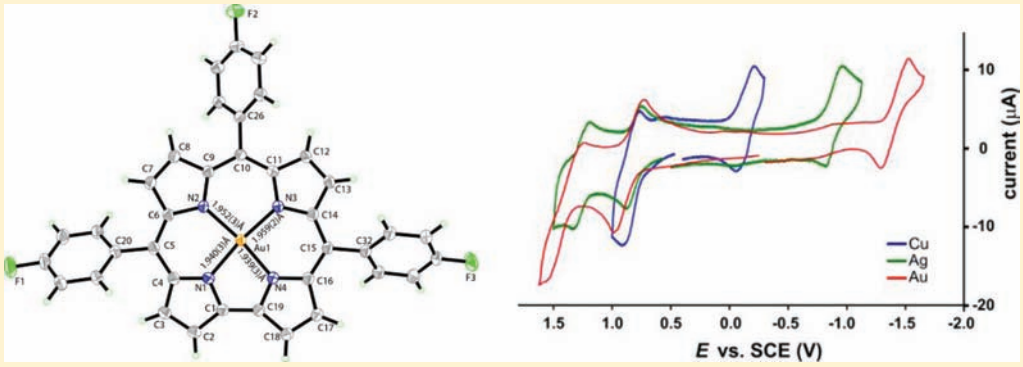

ABSTRACT: A number of third-row transition-metal corroles have remained elusive as synthetic targets until now, notably osmium, platinum, and gold corroles. Against this backdrop, we present a simple and general synthesis of β-unsubstituted gold(III) triarylcorroles and the first X-ray crystal structure of such a complex. Comparison with analogous copper and silver corrole structures, supplemented by extensive scalar-relativistic, dispersion-corrected density functional theory calculations, suggests that "inherent saddling" may occur for of all coinage metal corroles. The degree of saddling, however, varies considerably among the three metals, decreasing conspicuously along the series Cu > Ag > Au. The structural differences reflect significant differences in metal−corrole bonding, which are also reflected in the electrochemistry and electronic absorption spectra of the complexes. From Cu to Au, the electronic structure changes from noninnocent metal(II)−corrole(•2−) to relatively innocent metal(III)−corrole(3−).

INTRODUCTION

Despite the brisk pace of corrole research over the past decade, corroles continue to serve as platforms for novel coordination chemistry.[1] A number of third-row transition-metal corroles remain to be synthesized. Thus, although rhenium[2] and iridium[3] corroles have been synthesized, osmium, platinum, and gold corroles remain largely unexplored. In our laboratory, we have focused particularly on the problem of gold insertion into corroles.[4] Although β-octabromo-*meso*-triarylcorroles have proven amenable to gold insertion,[4,5] gold complexes of β-unsubstituted *meso*-triarylcorroles have remained elusive until now; thus, reagents such as chloroauric acid, $H[AuCl_4]\cdot H_2O$, were found to lead to uncontrolled β-chlorination and little actual gold insertion. Obliged to search for new routes to gold corroles, we decided to examine gold salts that lacked oxidatively transferable ligands such as chloride, a strategy that proved effective. Using gold(III) acetate, we have succeeded in synthesizing a family of β-unsubstituted gold(III) *meso*-triarylcorroles with systematically varying *meso*-aryl groups. Furthermore, single-crystal X-ray structure determinations could be obtained for the silver and gold complexes of *meso*-tris(*p*-fluorophenyl)corrole, [T(*p*-F)PC], permitting a detailed comparison with existing structural studies on copper corroles. The structural, electrochemical, and electronic absorption data, coupled with density functional theory (DFT) calculations,[6] have permitted a detailed comparative study of a full triad of coinage metal corroles. Despite superficial resemblance, the results indicate major variations in electronic character among the three coinage metals, when complexed with corroles.

RESULTS AND DISCUSSION

a. Synthesis and Proof of Composition. Gold(III) triarylcorroles were obtained by interaction of the free ligands and a moderate excess of gold(III) acetate in pyridine. The yields of about 30% were lower than those obtained for copper and silver corroles, which are typically >70%.[7] The complexes yielded mass and ^{1}H NMR spectra consistent with their expected structures (Figure 1). Temperature-dependent ^{1}H NMR spectra revealed no evidence of paramagnetic states, as are found for copper triarylcorroles.[8] Figure 1 depicts the room-temperature ^{1}H NMR spectrum of gold(III) *meso*-triphenylcorrole, Au[TPC], as a representative example.

b. Molecular Structures. X-ray-quality crystals proved difficult to obtain for the microcrystalline gold triarylcorroles.

Received: September 15, 2011
Published: November 23, 2011

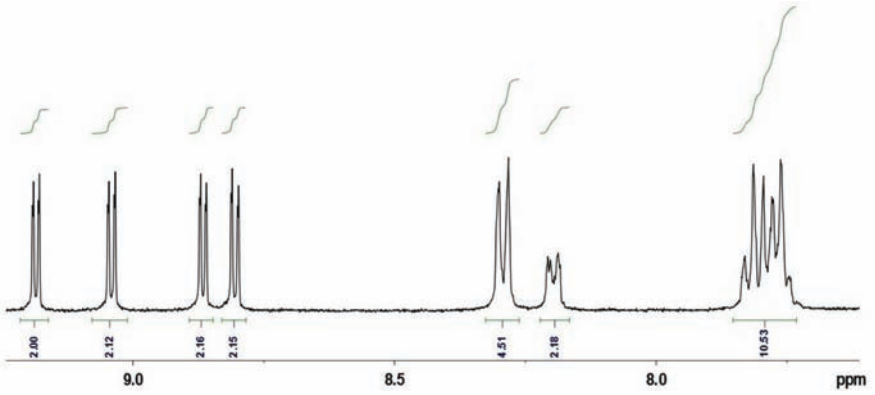

Figure 1. Room-temperature ^{1}H NMR spectrum of Au[TPC]. See the Experimental Section for assignments.

One of the complexes, Au[T(*p*-F)PC], however, lent itself to crystallographic analysis (Figure 2), providing the first such characterization for a simple β-unsubstituted gold corrole. The analogous silver structure could also be solved, and both these structures may be compared with a number of copper triarylcorrole crystal structures in the literature.[9] Key structural details, both experimental- and DFT-based, are presented in Table 1. A comparison of the gold and silver[10] structures shows that the Ag/Au−N distances are essentially identical (1.95−1.96 Å), but they are about 0.5−0.6 Å longer than the Cu−N distances.[11] Like copper corroles,[12,13] the silver and gold corrole structures reported herein are also saddled. Although common for metalloporphyrins, saddling is rare for metallocorroles and, as far as is known, unique to coinage metal corroles. In the case of metallocorroles, the saddling is believed to result from a metal($d_{x^2-y^2}$)−corrole("a_{2u}")[14] orbital interaction, which is symmetry-forbidden for a planar macrocycle geometry. Before proceeding further, however, it is useful to contextualize the issue of saddling vis-à-vis metallocorroles.

For metalloporphyrins, saddling most commonly occurs as a result of peripheral overcrowding;[15] it is thus particularly common for dodecasubstituted porphyrins and is essentially unknown for sterically unhindered porphyrins. The metal($d_{x^2-y^2}$)−porphyrin(a_{2u}) orbital interaction is well-established in such complexes. It explains, for instance, why saddled copper porphyrins are more easily oxidized relative to analogous saddled nickel porphyrins.[16] The same orbital interaction also accounts for the diamagnetism of saddled copper porphyrin π-cation-radical derivatives.[17] However, in none of these cases is the saddling a *result* of this orbital interaction. For metalloporphyrins, the $d_{x^2-y^2}$−a_{2u} interaction is undoubtedly strengthened by saddling; however, without exception, the saddling arises primarily as a result of peripheral steric crowding. Metallocorroles are different in this regard.

First, the $d_{x^2-y^2}$−"a_{2u}" interaction in coinage metal corroles results in saddling even in the absence of peripheral steric crowding. Second, even strong steric hindrance on the macrocycle periphery generally does not result in saddling in the absence of a suitable $d_{x^2-y^2}$−"a_{2u}" interaction. This is why saddling is generally not observed for noncoinage metal corroles. For example, whereas copper β-octabromo-*meso*-triarylcorroles are strongly saddled,[18,19] the analogous group 9 (cobalt, rhodium, and iridium) corroles are relatively planar.[3a,20] For metallocorroles, saddling thus directly reflects the mechanical power of the $d_{x^2-y^2}$−"a_{2u}" interaction and provides a unique window into ligand noninnocence.[21]

The degree of saddling varies considerably among corrole complexes formed by the three coinage metals. As shown in Table 1 and Figure 2, whereas β-unsubstituted copper triarylcorroles are very significantly saddled,[9a,12] with the saddling dihedral $\chi_3 \sim 45-55°$, Ag[T(*p*-F)PC] is less so ($\chi_3 \sim 38.8°$) and Au[T(*p*-F)PC] is even more flattened ($\chi_3 \sim 24.5°$). DFT (BP86-D[22,23]/STO-TZP)[24] calculations of saddling potentials (Figure 3) qualitatively reproduce these observations, confirming that gold corroles are much less saddled than their copper and silver analogues. Consistent with this picture, the crystal structure of Au[Br_8TPFPC] reported by Gross et al. also reveals an essentially planar corrole.[5]

An examination of the Kohn−Sham molecular orbitals (MOs; Figure 4) affords further insight into the comparative stereochemistry of the three coinage metals. The formally empty $d_{x^2-y^2}$ orbital of the "Cu(III)" center has a low orbital energy and avidly absorbs electron density from the corrole "a_{2u}" highest occupied molecular orbital (HOMO); copper corroles thus have significant copper(II)−corrole(•2−) character.[12,25] Observe from Figure 4a that both the HOMO and lowest unoccupied molecular orbital (LUMO) of Cu[TPC] involve $d_{x^2-y^2}$−"a_{2u}" interaction; they differ only in the relative phases of the $d_{x^2-y^2}$ and "a_{2u}" components. The low energy of the Cu $d_{x^2-y^2}$ orbital translates into a low HOMO−LUMO gap for copper triarylcorroles, consistent with an increasing population of paramagnetic states in the ^{1}H NMR spectra above room temperature.[8,9a] In the gold case, the high energy of the Au $5d_{x^2-y^2}$ orbital discourages significant mixing with the corrole a_{2u} HOMO; thus, as shown in Figure 4b, the HOMO of Au[TPC] has little Au $5d_{x^2-y^2}$ character. It follows that the HOMO−LUMO gap of Au[TPC] is much higher than that of Cu[TPC] and is comparable to that of a non-transition-metal porphyrinoid such as a typical zinc porphyrin; this may be seen from the energy level diagram shown in Figure 4c. In fact, the Au $5d_{x^2-y^2}$ orbital is so high in energy that it does not even correspond to the LUMO; for Au[TPC], it is actually the LUMO+2.

Like the majority of porphyrin and corrole crystal structures, coinage metal corroles show stacked macrocycles. For *C*2/*c*, the stacking is along the *c* axis. For the silver and gold structures reported herein, nearest-neighbor metal−metal distances are 3.8768(5) and 4.2294(5) Å for silver and 3.9296(4) and 4.3380(4) Å for gold. The corroles stack as inversion-related pairs, with a 2-fold axis and glide plane between two sets of pairs. The inversion-related pairs have the longer metal−metal distance, and the 2-fold/*c*-glide generates the shorter distance.

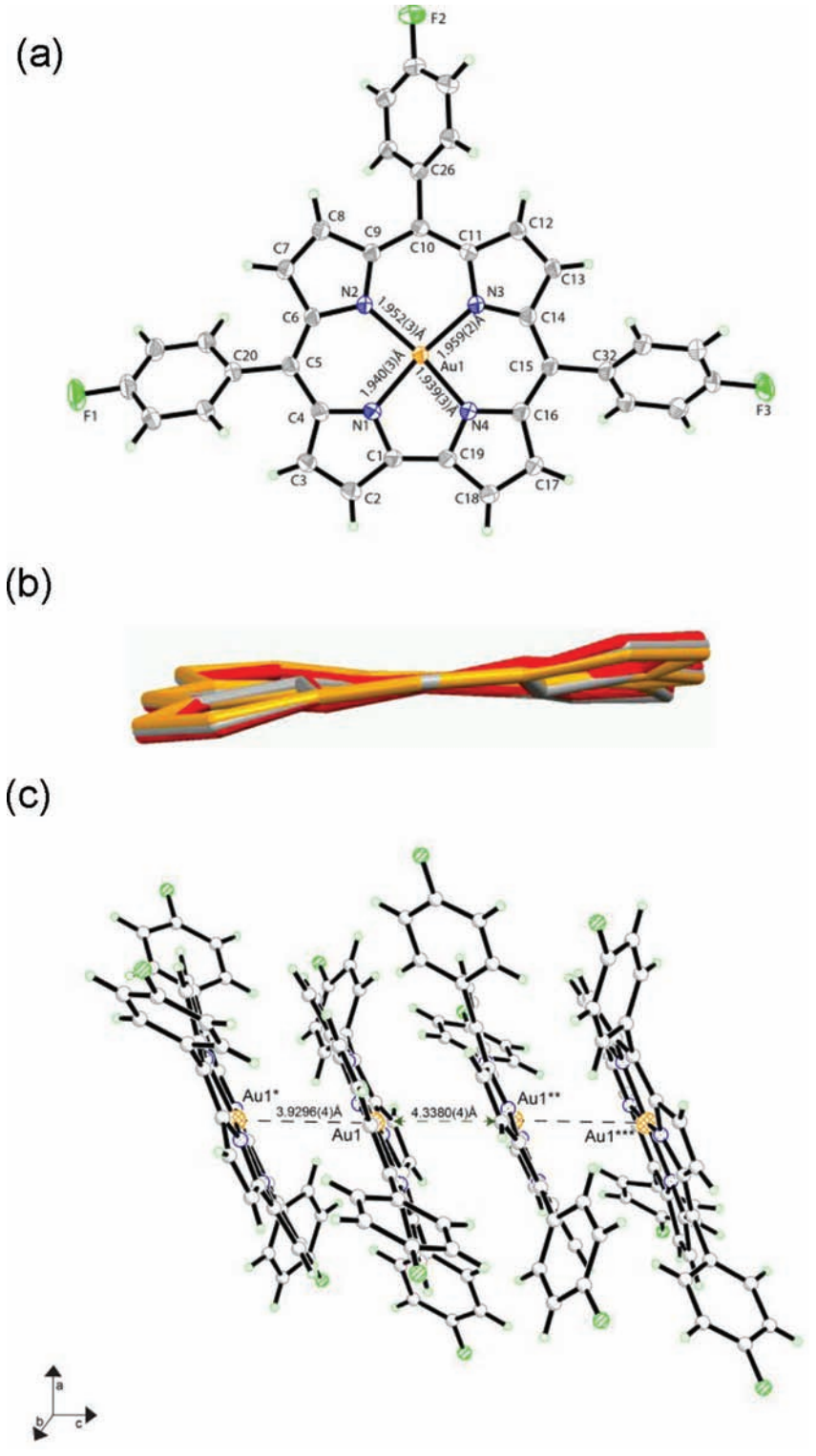

Figure 2. (a) Thermal ellipsoid (50%) diagram of Au[T(*p*-F)PC]. The disordered solvent was omitted for clarity. (b) Side-on view of copper (red), silver (gray), and gold (gold) corrole cores overlaid on one another. (c) Side view of corrole stacking.

The Au···Au distances are too long to be considered aurophilic interactions, which occur commonly for gold(I) compounds.[26]

c. Electrochemistry. Table 2 presents redox potentials for the various M[T(*p*-X)PC] (M = Cu, Ag, Au; X = CF_3, F, H, Me, OMe) complexes studied. Figure 5 presents cyclic voltammograms of the three M[T(*p*-F)PC] (M = Cu, Ag, Au) complexes. The results provide striking support for the MO picture presented above. Thus, whereas the first oxidation potentials vary little across the coinage metal triad, the reduction potentials vary dramatically, becoming increasingly negative down the triad. Stated differently, the electrochemical "HOMO−LUMO gaps" (defined as the algebraic difference between the first oxidation and reduction potentials) widen dramatically down the triad, in excellent agreement with our

dx.doi.org/10.1021/ic202023r | *Inorg. Chem.* 2011, 50, 12844–12851

Table 1. Selected Distances (Å) and Dihedral Angles (deg) for M[T(*p*-X−P)C] (M = Cu, Ag, Au) Crystal Structures[a]

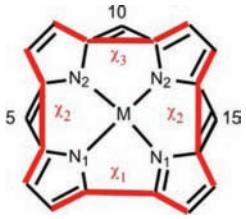

complex	M−N_1[b]	M−N_2[b]	χ_1	χ_2[b]	χ_3	source
Cu[TPC][c]	1.891 (1.889)	1.891 (1.901)	27.5 (25.3)	53.4 (47.7)	48.7 (42.7)	ref 9[c]
Ag[T(*p*-F−P)C]	1.943 (1.969)	1.955 (1.982)	19.9 (20.8)	38.8 (39.0)	38.8 (39.6)	this work
Au[T(*p*-F−P)C]	1.939 (1.960)	1.955 (1.978)	13.8 (7.3)	23.1 (18.3)	24.5 (21.3)	this work

[a]BP86-D values are shown in parentheses. [b]Average of two values for each experimental structure. [c]The metrical parameters reported in ref 12 are similar.

DFT calculations. A detailed spectroelectrochemical study has established that one-electron reduction of copper corroles is significantly metal-centered.[27] This is consistent with the nature of the LUMO shown in Figure 4a. According to our DFT calculations, Ag[TPC] too should undergo a similar, significantly metal-centered reduction. By contrast, our calculations indicate that, in the case of gold triarylcorroles, the reduction is exclusively corrole-centered.[28,29] Detailed electron paramagnetic resonance and Raman spectroelectrochemical studies are in progress to confirm these predictions, but the general agreement between the electrochemical and DFT-derived HOMO−LUMO gaps leaves little doubt about the qualitative correctness of our MO picture.

d. Electronic Absorption Spectra. Many metallotriarylcorrole families such as Cu, MnCl, and FeCl corroles exhibit strong meso-substituent effects on the Soret maxima (see Figure 6, inset, for the copper case). These have been analyzed in some detail for copper triarylcorroles and ascribed to so-called *hyper* character, i.e., phenyl-to-metal charge-transfer (CT) character mixing into the Soret transitions.[14] We have previously reported that such substituent effects are not observed for silver triarylcorroles,[14] and as shown in Figure 6, they are not observed for gold triarylcorroles either. The high HOMO−LUMO gaps in the silver and gold cases provide a natural explanation for the lack of CT character in their Soret bands.[16]

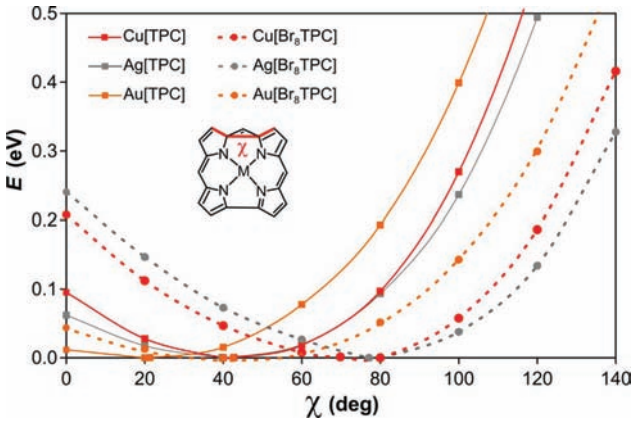

Figure 3. BP86-D saddling potentials for selected coinage metal corroles. Except for the saddling dihedral χ, all other internal coordinates have been optimized.

CONCLUDING REMARKS

In summary, we have presented a synthetic route to β-unsubstituted gold triarylcorroles and the first crystal structure of such a complex. Macrocycle saddling appears to be a common, structural feature of coinage metal corroles.[7−9,17] However, substantial variations in the degree of saddling, HOMO−LUMO gaps, and substituent effects on electronic absorption spectra reflect significant differences in metal−ligand bonding among the three coinage metals.[17] The experimental data, supported by DFT calculations, indicate that, as one moves down the triad, the electronic structure changes from a relatively noninnocent metal(II)−corrole(•2−) to an innocent metal(III)−corrole(3−) description.

EXPERIMENTAL SECTION

Instrumentation. UV−vis spectra were recorded on an HP 8453 spectrophotometer.

Cyclic voltammetry was performed with an EG&G model 263A potentiostat having a three-electrode system: a glassy carbon working electrode, a platinum wire counter electrode, and a saturated calomel reference electrode (SCE). Tetra(*n*-butyl)ammonium perchlorate (TBAP), recrystallized from absolute ethanol and dried in a desiccator for at least 1 week, was used as the supporting electrolyte. Anhydrous CH_2Cl_2 was used as the solvent. The reference electrode was separated from bulk solution by a fritted-glass bridge filled with the solvent/supporting electrolyte mixture. Pure argon was bubbled through the sample solutions for at least 5 min before the experiments were run. An argon blanket was maintained over the solutions while the experiments were in progress. All potentials were referenced to the SCE.

NMR spectra were recorded on a Mercury Plus Varian spectrometer (400 MHz for ^{1}H and 376 MHz for ^{19}F) at room temperature in $CDCl_3$. ^{1}H and ^{19}F shifts (δ) in ppm were referenced to residual chloroform (δ = 7.26) and 2,2,2-trifluoroethanol-d_3 (δ = −77.8), respectively.

Matrix-assisted laser desorption ionization time-of-flight (MALDI-TOF; α-cyano-4-hydroxycinnamic acid used as the matrix) and laser desorption ionization (LDI) mass spectra were recorded on a Waters Micromass MALDI micro MX mass spectrometer.

Materials. All reagents and solvents were used as purchased. Silica (DAVISIL LC150A 35−70 μm) was used for flash chromatography. Silica gel 60 preparative thin-layer chromatography (TLC) plates (20 cm × 20 cm, 0.5 mm thick, Merck) were used for further purification of some gold corroles for characterization purposes. Free base corroles H_3[T(*p*-X−P)C], where X = CF_3, F, H, CH_3, and OCH_3, were synthesized as described.[30]

Synthesis of Gold Triarylcorroles. A detailed procedure is given below for gold(III) 5,10,15-tris(4-fluorophenyl)corrole. Exactly the

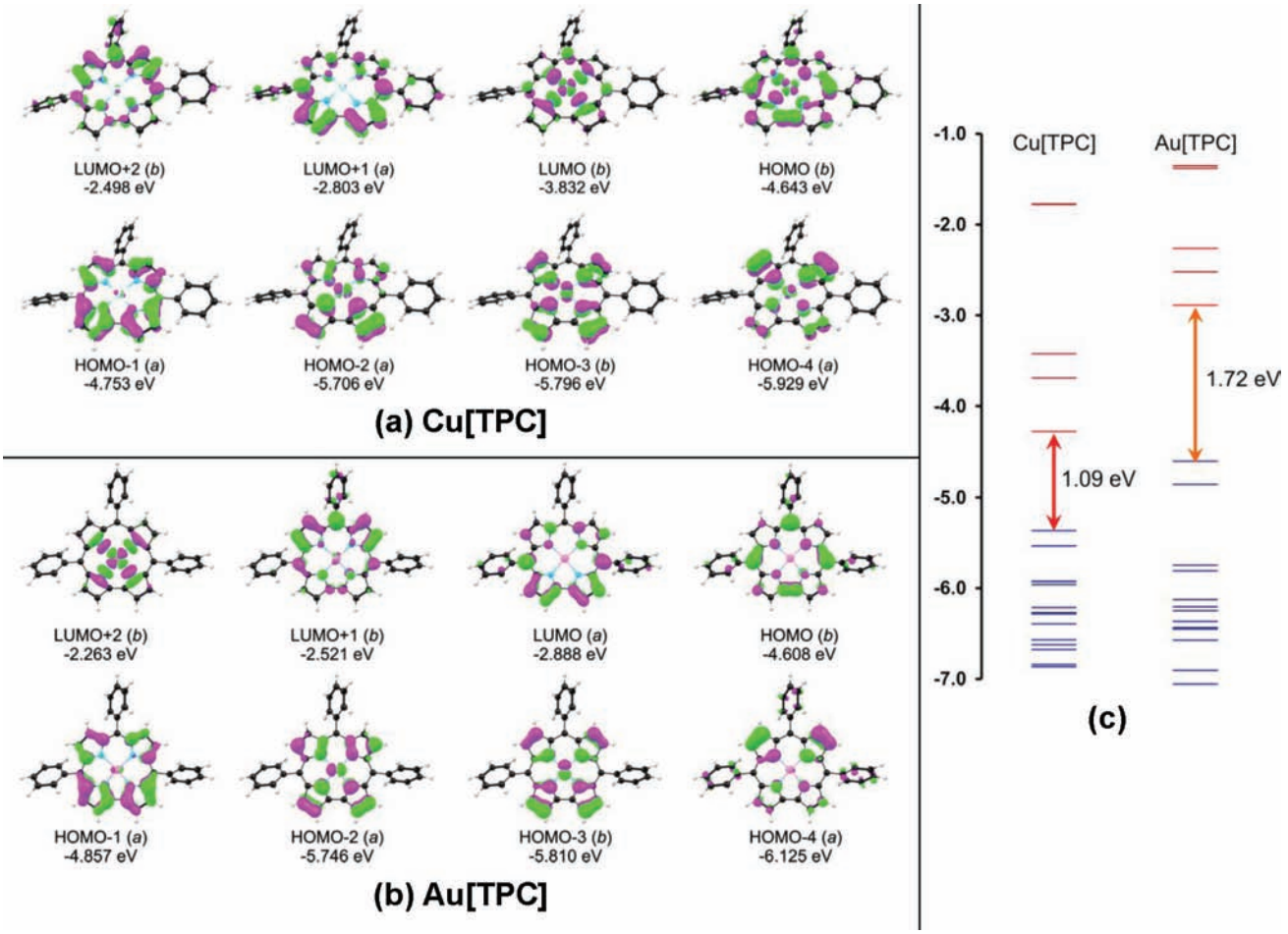

Figure 4. BP86/STO-TZP frontier MOs of (a) Cu[TPC] and (b) Au[TPC]. Also shown are C_2 irreducible representations and orbital energies. The MOs of Ag[TPC] are not shown because they are visually almost indistinguishable from those of Cu[TPC]. Part c shows the Kohn−Sham MO energy levels (eV) for the same two molecules, with the HOMO−LUMO gaps indicated.

same procedure is applicable for the other gold triarylcorroles reported herein, except for certain details of chromatographic purification, which varied for the different complexes and are therefore indicated separately.

Gold 5,10,15-(4-Fluorophenyl)corrole. To a 100-mL round-bottomed flask with H_3[T(*p*-F−P)C] (0.086 mmol, 50 mg) dissolved in 5 mL of pyridine was added 5 equiv of gold(III) acetate (161 mg, 0.43 mmol). The reaction mixture was stirred overnight for at least 16 h. The resulting reddish-brown mixture was rotary-evaporated, and the brown residue obtained was chromatographed on a silica gel column with 1:1 *n*-hexane/CH_2Cl_2. The gold corrole eluted as the first red band and was obtained as a dark-red solid after rotary evaporation.

Table 2. Half-Wave Potentials vs SCE ($E_{1/2}$, V) and Hammett ρ Values (mV) for M[T(*p*-X−P)C] in CH_2Cl_2 Containing 0.1 M TBAP (Scan Rate = 0.1 V s^{-1})

			oxidation		reduction		
M	X	3σ	first	second	first	ρ_{ox}	ρ_{red}
Cu	CF_3	1.62	0.89		−0.08[a]	97	69
	F	0.18	0.86		−0.13[b]		
	H	0.00	0.76		−0.20[a]		
	CH_3	−0.51	0.70		−0.23[a]		
	OCH_3	−0.81	0.65		−0.24[a]		
Ag	CF_3	1.62	0.91		−0.78[a]	105	51
	F	0.18	0.82	1.27	−0.87[b]		
	H	0.00	0.73		−0.86[a]		
	CH_3	−0.51	0.69		−0.88[a]		
	OCH_3	−0.81	0.66		−0.91[a]		
Au	CF_3	1.62	0.94		−1.29[b]	75	95
	F	0.18	0.85	1.38	−1.37[b]		
	H	0.00	0.80	1.35	−1.38[b]		
	CH_3	−0.51	0.78	1.35	−1.42[b]		
	OCH_3	−0.81	0.76	1.32	−1.57[b]		

[a]Alemayehu, A.; Conradie, J.; Ghosh, A. *Eur. J. Inorg. Chem.* **2011**, 1857−1864. [b]This work.

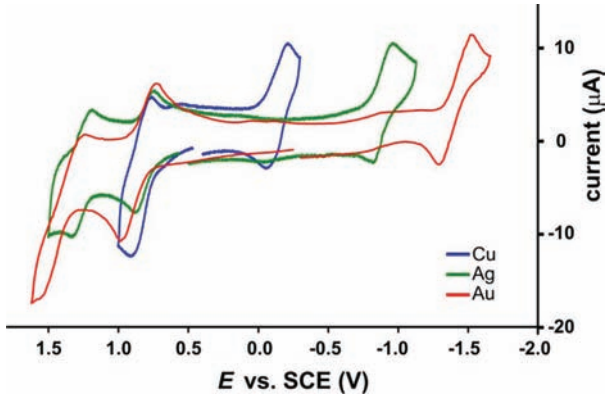

Figure 5. Cyclic voltammograms of M[T(*p*-F)PC] (M = Cu, Ag, Au) in CH_2Cl_2. See the Supporting Information for experimental details.

dx.doi.org/10.1021/ic202023r | *Inorg. Chem.* 2011, 50, 12844−12851

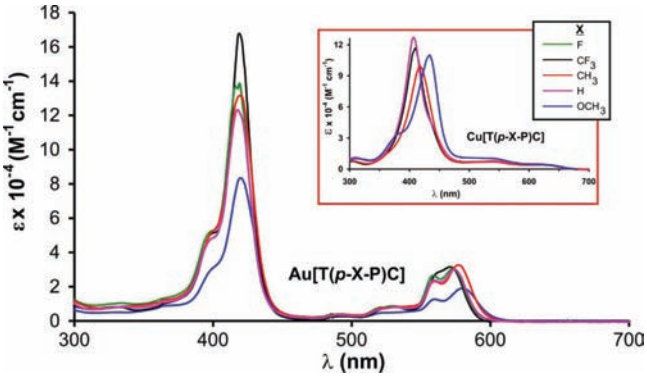

Figure 6. Electronic absorption spectra of Au[T(*p*-X−P)C] in CH_2Cl_2. Inset: spectra of Cu[T(*p*-X−P)C].

The complex was purified with preparative TLC using 13:7 *n*-hexane/CH_2Cl_2 as the eluent. Yield: 18 mg (27%). Dark-red needles suitable for X-ray analyses were obtained by the slow evaporation of a chloroform solution of the complex within 8 days. UV−vis (CH_2Cl_2): λ_{max}, nm ($\varepsilon \times 10^{-4}$, M^{-1} cm^{-1}) 419 (13.89), 530 (0.87), 559 (2.64), 573 (3.06). ^{1}H NMR: δ 9.20 (d, 2H, $^3J_{HH}$ = 4.4 Hz, β-H), 9.01 (d, 2H, $^3J_{HH}$ = 4.8 Hz, β-H), 8.84 (d, 2H, $^3J_{HH}$ = 4.4 Hz, β-H), 8.78 (d, 2H, $^3J_{HH}$ = 5.2 Hz, β-H), 8.24 (dd, 4H, $^3J_{HH}$ = 8.4 Hz, $^3J_{HF}$ = 5.6 Hz, 5,15-*o* or -*m*, Ph), 8.14 (dd, 2H, $^3J_{HH}$ = 8.4 Hz, $^3J_{HF}$ = 5.6 Hz, 10-*o* or -*m*, Ph), 7.56 − 7.44 (6H, 5,15-*m* or -*o* and 10-*m* or -*o*, Ph, overlapping triplets). ^{19}F NMR: δ −115.52 (m, 2F, 5,15-*p*-F, Ph), −115.60 (m, 1F, 10-*p*-F, Ph). MS (MALDI-TOF, major isotopomer): M^+ = 774.09 (expt), 774.54 (calcd for $C_{37}H_{20}N_4F_3Au$). Elem anal.: 57.19% C (calcd 57.38%), 2.48% H (calcd 2.60%), 7.10% N (calcd 7.23%).

Gold 5,10,15-Triphenylcorrole. Column chromatography on silica gel with 4:1 *n*-hexane/CH_2Cl_2 gave the complex as the first red eluate. Final purification was accomplished with preparative TLC, where 1:1 *n*-hexane/CH_2Cl_2 was used as the eluent, yielding the pure complex as the first red band. Yield: 17 mg (25%). UV−vis (CH_2Cl_2): λ_{max}, nm ($\varepsilon \times 10^{-4}$, M^{-1} cm^{-1}) 418 (12.31), 560 (2.37), 575 (2.99). ^{1}H NMR: δ 9.18 (d, 2H, $^3J_{HH}$ = 4 Hz, β-H), 9.04 (d, 2H, *J* = 4 Hz, β-H), 8.87 (d, 2H, $^3J_{HH}$ = 4 Hz, β-H), 8.81 (d, 2H, $^3J_{HH}$ = 4 Hz, β-H), 8.29 (d, 4H, $^3J_{HH}$ = 8 Hz, 5,15-*o* or -*m*, Ph), 8.20 (d, 2H, $^3J_{HH}$ = 8 Hz, 10-*o* or- *m*, Ph), 7.83−7.75 (m, 9H, 5,15-*m* or -*o*; 10-*m* or -*o*, and 5,10,15-*p*, Ph, overlapping). MS (MALDI-TOF, major isotopomer): M^+ = 720.57 (expt), 720.67 (calcd for $C_{37}H_{23}N_4Au$). Elem anal.: 61.38% C (calcd 61.67%), 3.10% H (calcd 3.22%), 7.65% N (calcd 7.78%).

Gold 5,10,15-Tris(4-trifluoromethylphenyl)corrole. Two successive chromatographic separations on silica gel columns with 3:2 *n*-hexane/CH_2Cl_2 yielded the complex as the first red eluate. Final purification was accomplished with preparative TLC, where 3:2 *n*-hexane/CH_2Cl_2 was used as the eluent, giving the complex as the first red band. Yield: 15 mg (24%). UV−vis (CH_2Cl_2): λ_{max}, nm ($\varepsilon \times 10^{-4}$, M^{-1} cm^{-1}) 419 (16.79), 530 (0.84), 571 (3.16). ^{1}H NMR: δ 9.17 (d, 2H, $^3J_{HH}$ = 4.4 Hz, β-H), 9.00 (d, 2H, $^3J_{HH}$ = 4.4 Hz, β-H), 8.81 (d, 2H, $^3J_{HH}$ = 4.8 Hz, β-H), 8.78 (d, 2H, $^3J_{HH}$ = 4.8 Hz, β-H), 8.38 (d, 4H, $^3J_{HH}$ = 8.0 Hz, 5,15-*m* or -*o*, Ph), 8.29 (d, 2H, $^3J_{HH}$ = 7.6 Hz, 10-*m* or -*o*, Ph), 8.09 (d, 4H, $^3J_{HH}$ = 7.6 Hz, 5,15-*o* or -*m*, Ph), 8.06 (d, 2H, $^3J_{HH}$ = 8.0 Hz, 10-*o* or -*m*, Ph). ^{19}F NMR: δ −62.53 (s, 9F, 5,10, 15-*p*-CF_3, Ph). MS (MALDI-TOF, major isotopomer): M^+ = 924.06 (expt), 924.57 (calcd for $C_{40}H_{20}N_4F_9Au$). Elem anal.: 52.12% C (calcd 51.96%), 2.44% H (calcd 2.18%), 5.77% N (calcd 6.06%).

Gold 5,10,15-Tris(4-methylphenyl)corrole. Silica gel chromatography with 4:1 *n*-hexane/CH_2Cl_2 gave the complex as the first red eluate. Final purification was accomplished with preparative TLC, where 1:1 *n*-hexane/CH_2Cl_2 was used as the eluent, giving the complex as the first red band. Yield: 24 mg (35%). UV−vis (CH_2Cl_2): λ_{max}, nm ($\varepsilon \times 10^{-4}$, M^{-1} cm^{-1}) 420 (13.16), 560 (2.31), 576 (3.25). ^{1}H NMR: δ 9.16 (d, 2H, *J* = 4 Hz, β-H), 9.05 (d, 2H, *J* = 8 Hz, β-H), 8.85 (d, 2H, *J* = 8 Hz, β-H), 8.81 (d, 2H, *J* = 8 Hz, β-H), 8.17 (d, 4H, *J* = 8 Hz, 5,15-*o* or -*m*, Ph), 8.08 (d, 2H, *J* = 8 Hz, 10-*o* or -*m*, Ph), 7.62 (d, *J* = 8 Hz, 4H, 5,15-*m* or -*o*, Ph), 7.58 (d, 2H, *J* = 8 Hz, 10-*m* or -*o*, Ph), 2.71 (s, 6H, 5, 15-*p*-CH_3), 2.70 (s, 3H, 10-*p*-CH_3). MS (MALDI-TOF, major isotopomer): M^+ = 762.65 (expt), 762.65 (calcd for $C_{40}H_{29}N_4Au$). Elem anal.: 62.69% C (calcd 62.99%), 3.83% H (calcd 3.83%), 7.27% N (calcd 7.35%).

Gold 5,10,15-Tris(4-methoxyphenyl)corrole. Silica gel chromatography with 2:3 *n*-hexane/CH_2Cl_2 gave the complex as the first red eluate. Yield: 16 mg (24%). UV−vis (CH_2Cl_2): λ_{max}, nm ($\varepsilon \times 10^{-4}$, M^{-1} cm^{-1}) 420 (8.34), 560 (1.26), 580 (1.92). ^{1}H NMR: δ 9.20 (d, 2H, $^3J_{HH}$ = 4.4 Hz, β-H), 9.05 (d, 2H, $^3J_{HH}$ = 5.2 Hz, β-H), 8.85 (d, 2H, $^3J_{HH}$ = 4.4 Hz, β-H), 8.82 (d, 2H, $^3J_{HH}$ = 4.8 Hz, β-H), 8.22 (d, 4H, $^3J_{HH}$ = 8.8 Hz, 5,15-*m* or -*o*, Ph), 8.11 (d, 2H, $^3J_{HH}$ = 8.8 Hz, 10-*m* or -*o*, Ph), 7.36 (d, 4H, $^3J_{HH}$ = 8.8 Hz, 5,15-*o* or -*m*, Ph), 7.32 (d, 2H, $^3J_{HH}$ = 8.8 Hz, 10-*o* or -*m*, Ph), 4.11 (s, 6H, 5,15-*p*-OCH_3, Ph), 4.10 (s, 3H, 10-*p*-OCH_3, Ph). MS (MALDI-TOF, major isotopomer): M^+ = 810.14 (expt), 810.65 (calcd for $C_{40}H_{29}N_4O_3Au$). Elem anal.: 58.98% C (calcd 59.26%), 3.55% H (calcd 3.61%), 6.89% N (calcd 6.91%).

Copper and Silver Corrole Syntheses. Copper and silver 5,10,15-tris(4-fluorophenyl)corroles were synthesized according to reported procedures.[7,9a] The latter was crystallized as dark-red needles by the slow evaporation of its chloroform solution within 1 week.

Copper 5,10,15-Tris(4-fluorophenyl)corrole. Yield: 84.6%. UV−vis (CH_2Cl_2): λ_{max}, nm ($\varepsilon \times 10^{-4}$, M^{-1} cm^{-1}) 413 (9.18), 539 (0.69), 615 (0.10). ^{1}H NMR: δ 7.92 (d, 2H, $^3J_{HH}$ = 4 Hz, β-H), 7.75 (dd, 4H, $^3J_{HH}$ = 8 Hz, $^3J_{HF}$ = 5.6 Hz, 5,15-*o* or -*m*, Ph), 7.68−7.62 (m, 4H, β-H and 10-*o* or -*m*, Ph), 7.34 (d, 2H, $^3J_{HH}$ = 4 Hz, β-H), 7.24−7.25 (m, 8H, β-H, 10-*m* or -*o*, Ph and 5,15-*m* or -*o*, Ph, overlapping). ^{19}F NMR: δ −112.64 (m, 2F, 5,15-*p*-F, Ph), −112.95 (m, 1F, 10-*p*-F, Ph). MS (MALDI-TOF, major isotopomer): M^+ = 640.13 (expt), 641.12 (calcd for $C_{37}H_{20}N_4F_3Cu$). Elem anal.: 69.66% C (calcd 69.32%), 3.28% H (calcd 3.14%), 8.89% N (calcd 8.74%).

Silver 5,10,15-Tris(4-fluorophenyl)corrole. Yield: 70%. UV−vis (CH_2Cl_2): λ_{max}, nm ($\varepsilon \times 10^{-4}$, M^{-1} cm^{-1}) 422(11.53), 522 (0.75), 563 (0.32), 581 (3.30). ^{1}H NMR: δ 9.21 (d, 2H, $^3J_{HH}$ = 4 Hz, β-H), 8.93 (d, 2H, $^3J_{HH}$ = 4.8 Hz, β-H), 8.73 (d, 2H, $^3J_{HH}$ = 4.8 Hz, β-H), 8.71 (d, 2H, $^3J_{HH}$ = 4.4 Hz, β-H), 8.26 (dd, 4H, $^3J_{HH}$ = 8.8 Hz, $^3J_{HF}$ = 5.6 Hz, 5,15-*o* or -*m*, Ph), 8.16 (dd, 2H, $^3J_{HH}$ = 8.8 Hz, $^3J_{HF}$ = 5.6 Hz, 10-*o* or -*m*, Ph), 7.56−7.44 (6H, 5,15-*m* or -*o* and 10-*m* or -*o*, Ph, overlapping triplets). ^{19}F NMR: δ −115.38 (m, 2F, 5,15-*p*-F, Ph), −115.53 (m, 1F, 10-*p*-F, Ph). MS (LDI-TOF, major isotopomer): M^+ = 686.08 (expt), 685.45 (calcd for $C_{37}H_{20}N_4F_3Ag$). Elem anal.: 65.10% C (calcd 64.83%), 3.05% H (calcd 2.94%), 8.35% N (calcd 8.17%).

Crystallographic Analysis of Au[T(*p*-F−P)C]·0.5C_6H_{14}. A dark-red needle of dimensions 0.35 × 0.04 × 0.04 mm^3 was mounted in the 100(2) K nitrogen cold stream provided by an Oxford Cryostream low-temperature apparatus on the goniometer head of a Bruker D85 diffractometer equipped with an Apex II CCD detector, on beamline 11.3.1 at the Advanced Light Source in Berkeley, CA. Diffraction data were collected using synchrotron radiation monochromated with silicon(111) to a wavelength of 0.774 90(1) Å. A full sphere of data was collected using 0.3° ω scans. A multiscan absorption correction was applied using the program *SADABS 2008/1*. The data consist of 48 038 reflections collected, of which 10 431 were unique [*R*(int) = 0.0563] and 9238 were observed [$I > 2\sigma(I)$]. The structure was solved by direct methods (*SHELXS*) and refined by full-matrix least squares on F^2 (*SHELXL-97*) using 455 parameters and 28 restraints. The solvent, hexane, is disordered. Two orientations were identified and refined. Because of the overlapping of the two orientations, distance 1−2 and 1−3 restraints were used to control the hexane geometries. The hydrogen atoms on carbon atoms were generated geometrically and refined as riding atoms with C−H = 0.95−0.99 Å and U_{iso}(H) = 1.2U_{eq}(C) for CH and CH_2 groups and U_{iso}(H) = 1.5U_{eq}(C) for CH_3 groups. The maximum and minimum peaks in the final difference Fourier map were 1.599 and −1.291 e $Å^{-3}$. Crystal data: $C_{40}H_{27}F_3N_4Au$, M_w = 817.62, monoclinic, *C*2/*c*, *a* = 21.0234(17) Å, *b* = 19.9239(16) Å, *c* = 15.8500(13) Å, α = 91.4200(10)°, *V* = 6637.0(9) $Å^3$, *T* = 100(2) K, *Z* = 8, R1 [$I > 2\sigma(I)$] = 0.0311, wR2 (all data) = 0.0955, GOF (on F^2) = 1.030.

Crystallographic Analysis of Ag[T(*p*-F−P)C]·$CHCl_3$. A dark-red block of dimensions 0.05 × 0.03 × 0.02 mm^3 was mounted as described above, on beamline 11.3.1 at the Advanced Light Source in

Berkeley, CA. Diffraction data were collected and processed in the method described above. The data consist of 47 883 reflections collected, of which 9866 were unique [R(int) = 0.0558] and 7634 were observed [$I > 2\sigma(I)$]. The structure was solved by direct methods (*SHELXS*) and refined by full-matrix least squares on F^2 (*SHELXL-97*) using 442 parameters and 0 restraints. The hydrogen atoms on carbon atoms were generated geometrically and refined as riding atoms as described above. The maximum and minimum peaks in the final difference Fourier map were 1.283 and −2.000 e Å^{-3}. Crystal data: $C_{38}H_{21}F_3N_4Cl_3Ag$, M_w = 804.81, monoclinic, $C2/c$, a = 20.2684(9) Å, b = 20.2432(9) Å, c = 15.6451(7) Å, α = 90.478(3)°, V = 6418.9(5) Å^3, T = 100(2) K, Z = 8, R1 [$I > 2\sigma(I)$] = 0.0516, wR2 (all data) = 0.1437, GOF (on F^2) = 1.029.

DFT Calculations. All calculations were carried out with the *ADF 2009* program system. The dispersion-corrected BP86-D functional was used throughout, and scalar relativistic effects were taken into account with the ZORA Hamiltonian and ZORA STO-TZP basis sets. Fine integration grids and tight criteria for self-consistent-field and geometry optimization were used to ensure accurate geometries and saddling potential curves.

■ ASSOCIATED CONTENT

Ⓢ Supporting Information

DFT-optimized coordinates and a combined CIF file. This material is available free of charge via the Internet at http://pubs.acs.org.

■ AUTHOR INFORMATION

Corresponding Author

*E-mail: abhik.ghosh@uit.no.

■ ACKNOWLEDGMENTS

This work was supported by the Research Council of Norway. The Advanced Light Source is supported by the Director, Office of Science, Office of Basic Energy Sciences, of the U.S. Department of Energy under Contract No. DE-AC02-05CH11231. J.C. acknowledges the National Research Fund of the Republic of South Africa.

■ REFERENCES

(1) For a recent review, see: Aviv-Harel, I.; Gross, Z. *Chem.—Eur. J.* **2009**, *15*, 8382−8394.

(2) Tse, M. K.; Zhang, Z.; Mak, T. C. W.; Chan., K. S. *J. Chem. Soc., Chem. Commun.* **1998**, 1199−1200.

(3) (a) Palmer, J. H.; Day, M. W.; Wilson, A. D.; Henling, L. M.; Gross, Z.; Gray, H. B. *J. Am. Chem. Soc.* **2008**, *130*, 7786−7787. (b) Palmer, J. H.; Durrell, A. C.; Gross, Z.; Winkler, J. R.; Gray, H. B. *J. Am. Chem. Soc.* **2010**, *132*, 9230−9231.

(4) Alemayehu, A.; Ghosh, A. *J. Porphyrins Phthalocyanines* **2011**, *15*, 106−110.

(5) While this paper was under review, a report of gold(III) β-octabromo-*meso*-tris(pentafluorphenyl)corrole, Au[Br$_8$TPFPC], including an X-ray crystal structure, appeared in the literature: Rabinovitch, E.; Goldberg, I.; Gross, Z. *Chem.—Eur. J.* **2011**, *17*, 12294−12301.

(6) Reviews on DFT studies of porphyrins and related compounds: (a) Ghosh, A. *Acc. Chem. Res.* **1998**, *31*, 189−198. (b) Ghosh, A. In *The Porphyrin Handbook*; Kadish, K. M., Guilard, R., Smith, K. M., Eds.; Academic: San Diego, 1999; Vol. 7, Chapter 47, pp 1−38. (c) Ghosh, A.; Steene, E. *J. Biol. Inorg. Chem.* **2001**, *6*, 739−752. (d) Ghosh, A. *J. Biol. Inorg. Chem.* **2006**, *11*, 712−724.

(7) Wasbotten, I. H.; Wondimagegn, T.; Ghosh, A. *J. Am. Chem. Soc.* **2002**, *124*, 8104−8116.

(8) Steene, E.; Wondimagegn, T.; Ghosh, A. *J. Am. Chem. Soc.* **2003**, *125*, 16300−16309.

(9) For key early examples of copper corrole X-ray structures, see: (a) Brückner, C.; Brinas, R. P.; Bauer, J. A. K. *Inorg. Chem.* **2003**, *42*, 4495−4497. (b) Luobeznova, I.; Simkhovich, L.; Goldberg, I.; Gross, Z. *Eur. J. Inorg. Chem.* **2004**, 1724−1732. (c) Bröring, M.; Bregier, F.; Tejero, E. C.; Hell, C.; Hell, C.; Holthausen, M. C. *Angew. Chem., Int. Ed.* **2007**, *46*, 445−448.

(10) For other examples of silver corrole X-ray structures, see: (a) Pacholska, E.; Espinosa, E.; Guilard, R. *Dalton Trans.* **2004**, 3181−3183. (b) Brückner, C.; Barta, C. A.; Brinas, R. P.; Bauer, J. A. K. *Inorg. Chem.* **2003**, *42*, 1673−1680. (c) Stefanelli, M.; Mastroianni, M.; Nardis, S.; Licoccia, S.; Fronczek, F. R.; Smith, K. M.; Zhu, W.; Ou, Z.; Kadish, K. M.; Paolesse, R. *Inorg. Chem.* **2007**, *46*, 10791−10799.

(11) The fact that these distances are all fairly similar is dictated by the steric constraints of the corrole macrocycle. The fact that the bond distances involving silver and gold are similar is explained by their similar ionic radii, 0.89 and 0.99 Å, respectively, for the 3+ ions, which may be compared with significantly smaller values of 0.54 Å for Cu^{III} and 0.73 Å for Cu^{II}: Shannon, R. D. *Acta Crystallogr.* **1976**, *A32*, 751−767.

(12) The fact that copper corroles are *inherently*[11] saddled was first noted in: Alemayehu, A. B.; Gonzalez, E.; Hansen, L.-K.; Ghosh, A. *Inorg. Chem.* **2009**, *48*, 7794−7799.

(13) The term "inherent" or "intrinsic" refers to the fact that the saddling is driven primarily by metal−ligand orbital interactions and not by peripheral substituents, although the latter can accentuate the saddling. The term "intrinsic ruffling" has been used for nickel porphyrins: Kozlowski, P. M.; Rush, T. S.; Jarzecki, A. A.; Zgierski, M. Z.; Chase, B.; Piffat, C.; Ye, B.-H.; Li, X.-Y.; Pulay, P.; Spiro, T. G. *J. Phys. Chem. A* **1999**, *103*, 1357−1366.

(14) The two HOMOs of corrole, a_2 and b_1 in C_{2v} symmetry, are very similar in shape to the porphyrin a_{1u} and a_{2u} HOMOs, respectively. We will therefore continue to use the D_{4h} porphyrin irreps to describe the corrole HOMOs: Ghosh, A.; Wondimagegn, T.; Parusel, A. B. J. *J. Am. Chem. Soc.* **2000**, *122*, 5100−5104.

(15) For reviews on nonplanar porphyrins, see: (a) Senge, M. *Chem. Commun.* **2006**, 243−256. (b) Shelnutt, J. A.; Song, X. Z.; Ma, J. G.; Jia, S. L.; Jentzen, W.; Medforth, C. J. *Chem. Soc. Rev.* **1998**, *27*, 31−41.

(16) Ghosh, A.; Halvorsen, I.; Nilsen, H. J.; Steene, E.; Wondimagegn, T.; Lie, E.; van Caemelbecke, E.; Guo, N.; Ou, Z.; Kadish, K. M. *J. Phys. Chem. B* **2001**, *105*, 8120−8124.

(17) (a) Renner, M. W.; Barkigia, K. M.; Zhang, Y.; Medforth, C. J.; Smith, K. M.; Fajer, J. *J. Am. Chem. Soc.* **1994**, *116*, 8582−8592. (b) Renner, M. W.; Barkigia, K. M.; Fajer, J. *Inorg. Chim. Acta* **1997**, *263*, 181−187.

(18) Alemayehu, A.; Hansen, L. K.; Ghosh, A. *Inorg. Chem.* **2010**, *49*, 7608−7610.

(19) The most strongly saddled metallocorrole reported to date is a copper β-octakis(trifluoromethyl)-*meso*-triarylcorrole: Thomas, K. E.; Hansen, L. K.; Conradie, J.; Ghosh, A. *Eur. J. Inorg. Chem.* **2011**, 1865−1870.

(20) Paolesse, R.; Nardis, S.; Sagone, F.; Khoury, R. G. *J. Org. Chem.* **2001**, *66*, 550−556.

(21) Ligand noninnocence is ubiquitous for metallocorroles. For key studies, see: (a) Cai, S.; Walker, F. A.; Licoccia, S. *Inorg. Chem.* **2000**, *39*, 3466−3478. (b) Steene, E.; Wondimagegn, T.; Ghosh, A. *J. Phys. Chem. B* **2001**, *105*, 11406−11413; Addition/correction: *J. Phys. Chem. B* **2002**, *106*, 5312. (c) Zakharieva, O.; Schünemann, V.; Gerdan, M.; Licoccia, S.; Cai, S.; Walker, F. A.; Trautwein, A. X. *J. Am. Chem. Soc.* **2002**, *124*, 6636−6648. (d) Nardis, S.; Paolesse, R.; Licoccia, S.; Fronczek, F. R.; Vicente, M. G. H.; Shokhireva, T. K.; Cai, S.; Walker, F. A. *Inorg. Chem.* **2005**, *44*, 7030−7046. (e) Walker, F. A.; Licoccia, S.; Paolesse, R. *J. Inorg. Biochem.* **2006**, *100*, 810−837. (f) Roos, B. O.; Veryazov, V.; Conradie, J.; Taylor, P. R.; Ghosh, A. *J. Phys. Chem.* **2008**, *112*, 14099−14102. (g) Kadish, K. M.; Shen, J.; Fremond, L.; Chen, P.; Ojaimi, M. E.; Chkounda, M.; Gros, C. P.; Barbe, J.-M.; Ohkubo, K.; Fukuzumi, S.; Guilard, R. *Inorg. Chem.* **2008**, *47*, 6726−6737.

(22) (a) Becke, A. D. *Phys. Rev.* **1988**, *A38*, 3098−3100. (b) Perdew, J. P. *Phys. Rev.* **1986**, *B33*, 8822. Erratum: Perdew, J. P. *Phys. Rev.* **1986**, *B34*, 7406.

(23) Grimme, S.; Antony, J.; Ehrlich, S.; Krieg, H. *J. Chem. Phys.* **2010**, *132*, 154104−154119.

(24) The ADF program system uses methods described in: Velde, G. T.; Bickelhaupt, F. M.; Baerends, E. J.; Guerra, C. F.; Van Gisbergen, S. J. A.; Snijders, J. G.; Ziegler, T. *J. Comput. Chem.* **2001**, *22*, 931−967.
(25) The noninnocent nature of copper corroles has been confirmed by ab initio CASPT2 calculations: Pierloot, K.; Zhao, H.; Vancoillie, S. *Inorg. Chem.* **2010**, *49*, 10316−10329.
(26) For a recent study, see: Assadollahzadeh, B.; Schwerdtfeger, P. *Chem. Phys. Lett.* **2008**, *462*, 222−228.
(27) Ou, Z.; Shao, J.; Zhao, H.; Ohkubo, K.; Wasbotten, I. H.; Fukuzumi, S.; Ghosh, A.; Kadish, K. M. *J. Porphyrins Phthalocyanines* **2004**, *8*, 1236−1247.
(28) The Hammett analyses included in Table 2 do not appear to be particularly valuable in this regard. The various ρ's are all rather similar,[24] suggesting that the various redox processes have comparable amounts of corrole-centered character. Our MO picture is consistent with this conclusion, even though in the copper and silver cases the LUMOs have significant metal character as well and the reductions are partially metal-centered.
(29) Much higher ρ's have been measured for copper β-octakis-(trifluoromethyl)-*meso*-triarylcorroles:[17] Thomas, K. E.; Wasbotten, I. H.; Ghosh, A. 2008, *47*, 10469−10478. Addition/correction: *Inorg. Chem.* **2009**, *48*, 1257−1257.
(30) Koszarna, B.; Gryko, D. T. *J. Org. Chem.* **2006**, *71*, 3707−3717.